On the effects of convecting entropy waves on the combustor hydrodynamics

S. M. Hosseinalipour[1*], A. Fattahi[1], H. Afshari[1], N. Karimi[2]

[1]School of Mechanical Engineering, Iran University of Science and Technology, Tehran, Iran
[2]School of Engineering, University of Glasgow, Glasgow G12 8QQ, United Kingdom
* Corresponding author: asmostef@gmail.com

Abstract

Entropy waves, as hot spots or density inhomogeneities, can be generated by the flame unsteadiness in combustors. These waves are convected downstream while being annihilated by the flow decay and dispersion mechanisms. This results in the diffusion of the enthalpy of the wave within the base flow. Decaying entropy waves may, therefore, affect the density and viscosity of the base flow and consequently modify the combustor hydrodynamics. Study of such hydrodynamic modifications is the objective of the current numerical study. In particular, the extent of induced changes in the flow is investigated. To do so, some hydrodynamic indices are introduced, in which vorticity magnitude and the angles between the velocity and vorticity vectors are the main parameters. In keeping with the previous studies, entropy waves are inserted at the channel inlet by a linear-increment and exponential-decrement temperature function in a cold flow. A more realistic, and rarely investigated thermal boundary condition of convective type are considered on the walls of the channel. The results show that convection of the entropy waves through the channel noticeably changes the hydrodynamic parameters, such as vorticity vector, helicity and streamlines alignment. This is in contrast with the general notion, which regards entropy waves as passive scalars.

Keywords: Convecting entropy waves; Combustor hydrodynamics; Streamline wrapping and coiling; Vorticity and helicity vector.

Introduction

Nomenclature			
CFL	Courant-Friedrichs-Lewy number	**Greek symbols**	
h	Channel half-height	γ	Heat capacity ratio
h_s	Sensible enthalpy	λ	Thermal conductivity
k	Turbulent kinetic energy	μ	Dynamic viscosity
p	Pressure	υ	kinematic viscosity
Re	Reynolds number	ρ	density
S	Strain rate	τ	Shear stress
t	Time	**Subscripts and superscripts**	
T	Temperature	max	Maximum
u	Velocity	res	Resolved domain
V	Volume of a computational cell	tot	Total
$\forall$	Computational domain	w	Pertaining to wall
		τ	Pertaining to turbulence

Combustion generated noise is an important source of noise in power generating devices, such as gas turbines and aero-engines [1,2]. Reduction of this noise source is of significance from the environmental point of view [3]. Combustion noise may, further, contribute with the so called thermoacoustic instabilities in combustors [2,4]. These instabilities often include strong pressure oscillations, which can induce pronounced thermal stresses and mechanical vibrations and therefore lead to hardware damage [4]. Avoiding thermoacoustic instabilities and reducing the noise level are, currently, amongst the major challenges before the development of clean and quiet gas turbines [4].

Addressing these issues requires a deep understanding of all the relevant physical processes that can influence the problem of combustion noise.

Conventionally, combustion noise is attributed to the interactions between flow turbulence and the flame heat release [1]. This is usually regarded as direct combustion noise [1]. In addition to this, there exists a second mechanism of noise generation in reactive flows, referred to as indirect combustion noise or entropy noise [1]. This is a lesser explored mechanism in comparison with direct noise. Nonetheless, there is now strong evidence indicating that entropy noise could be the main source of combustion noise in gas turbines [5,6,7]. This is the reason of increasing emphasis on understanding entropy waves as the main component of indirect combustion noise. Entropy waves are density inhomogeneities or hot spots, resulting from unsteady combustion [1]. In combustors, they can be produced by the interactions between the flame and acoustics and the subsequent combustion of the unburned fuel packs downstream of the flame [4,8]. This leads to the development of a front with a higher temperature compared with that of the base flow, which is often regarded as entropy wave [1,2]. The wave is then convected throughout the combustor by the mean flow and is partially converted to acoustic waves in a downstream nozzle or diffuser [4]. This should be noted that the term convection indicates the displacement of the entropy wave by the mean flow. The physical principles of entropy noise were, first, explained by Ffowcs Williams and Howe [9] and Howe [10]. Later, the process of conversion of entropy waves to acoustic waves was modelled by Marble and Candel [11]. This work included a linear analysis of a one-dimensional non-diffusive flow. Recently, the work of Marble and Candel has been extended to nonlinear cases in a series of theoretical and numerical works by a number of authors [12-14]. Although significant advances were made in these studies, the interactions among entropy wave and the convective base flow and the thermal influences of the flow boundaries were largely ignored.

In practice, the generation of entropy noise includes convection of flame generated density inhomogeneities (entropy waves) towards the exit nozzle. During this convection process, entropy waves are subject to viscous dissipation, turbulent mixing and flow non-uniformities. These effects can lead to a partial or complete wave annihilation and hence, eliminate the noise source. Some experimental measurements of entropy waves inside thermoacoustically unstable combustors have confirmed that entropy waves could be highly dispersive [14, 15]. Nevertheless, most existing analytical [11,16,17], numerical [2,18,19] and experimental [1,20-22] works have neglected this. Only a few studies considered entropy wave dissipation and dispersion [23-25]. Eckstein et al [23, 24] considered the dispersion of entropy waves and argued that entropy waves make a negligible contribution with the thermoacoustic instability of the combustor [24]. Their model for the dispersion of entropy wave was developed in the earlier work of Sattelmayer [25], who modelled the dispersing process as a temporal stretch of a density impulse. This analysis was on the basis of the residence time distribution in a simple exhaust duct [25]. Sattelmayer [25] argued that non-uniformity of a duct flow could cause significant dispersion and hence, entropy waves could hardly survive in real combustors. He, therefore, considered entropy waves to be of little significance in the analysis of thermoacoustic instabilities and combustion noise [25]. In sharp contrast with this conclusion, recent direct numerical simulation of Morgans et al. [26], in an incompressible non-reactive channel flow, showed that entropy waves could mostly survive the flow decay and dispersion effects. Nonetheless, Morgans et al. confirmed the effects of shear dispersion on the entropy wave. This is predominantly due to non-uniformity of a fully-developed velocity profile. Regardless of the ongoing debates on the strength of entropy wave dissipation in combustors, it is clear that these waves are subject to some levels of dissipation.

Although there have been a few efforts to investigate the effects of flow field on entropy waves [23-27], there is, currently, no study on the contrariwise effects. By dissipation of the hot parcels in the flow, heat diffuses into the base convective flow and modifies the fluid density and subsequently alters the velocity and vorticity fields. These hydrodynamic modifications are, then, likely to affect the combustor acoustics through mechanisms of aerodynamic noise [26,27]. However, currently, there is no measure of such hydrodynamic modifications. Further, the thermal boundary conditions of the combustor can act as a crucial parameter affecting the dissipation of entropy waves. In reality, the thermal boundary condition of a gas turbine combustor is of convective types due to the flow of bypass air on the combustor external walls. Yet, such thermal boundary conditions have been rarely considered in the analysis of entropy waves. Thus, the influences of realistic thermal boundary

conditions on the entropy wave dissipation and subsequently combustor hydrodynamics have remained totally unexplored. By considering adiabatic and convective thermal boundary conditions, the current work investigates the flow modifications induced by the convection and annihilation of entropy waves in a channel. The process of entropy wave convection is analyzed through large eddy simulation (LES) of a fully developed flow between two parallel plates. Some hydrodynamic indicators are, then, introduced to evaluate the influences of entropy wave on the base flow. It is found that the annihilation of entropy wave noticeably modifies the hydrodynamics of the convective flow.

2. Problem configuration and Numerical method

2.1. Geometry and boundary conditions

A fully-developed turbulent flow between two parallel plates, similar to that of Morgans et al. [26], is considered, see Fig. 1. The computational length, height and width are respectively $24\pi h$, $2h$ and πh.

Take in Fig. 1

The turbulent Reynolds number, defined as

$$Re_\tau = u_\tau h/\upsilon, \quad (1)$$

is assumed to be 180, similar to Morgans et al. [26], in which h is the channel half-height, υ is the kinematic viscosity and u_τ is the friction velocity, described as follows.

$$u_\tau = \sqrt{\frac{\tau_w}{\rho}}, \quad (2)$$

where, τ_w is the shear stress on the wall. Reynolds number based on hydraulic diameter and bulk velocity is assumed to be 7500 and 13000, while this is based on h (Fig. 1) and centerline velocity is 1700 and 3400. These are hereafter called respectively $0.5Re_{max}$ and Re_{max}. Fully-developed velocity profile at the inlet, periodic boundary condition in the spanwise direction and no-slip condition on the walls are applied. Fully-developed inlet velocity profile is numerically obtained at the outlet of the channel, which is longer than the hydrodynamic entrance length [28]. It is also statistically found that the deviation of the velocity profile through the channel from the fully-developed inlet condition is negligible. At the outlet, zero axial gradients for all flow variables are imposed [26]. Either adiabatic or convective thermal boundary conditions are employed on the walls. The value of the heat transfer coefficient and free stream temperature are 100 W/m^{2}K and 273 K, respectively, for a typical aero-combustor [29]. The inlet temperature is kept constant at 300K and the working fluid is assumed to be air.

2.2. Governing equations and numerical methods

In the current problem, eddies can have crucial effects upon the dissipation and dispersion of entropy waves. Thus, at least, large eddies should be accurately simulated. Numerical simulations of Reynolds average Navier-Stokes (RANS) equations cannot capture eddies and only model them via Reynolds stress terms. On the other hand, DNS is prohibitively expensive for the case studies in the current problem. Therefore, large eddy simulation (LES) is employed in this investigation.

The governing equations in LES are obtained by filtering the Navier-Stokes equations upon the physical domain. Filtered equations can effectively separate large and small scale eddies. Filtering, similar to equations of RANS, adds a term to the momentum equation. This is the subgrid-scale stress which is unknown and requires modeling.

Quantity of φ is decomposed into large-scale $\bar{\varphi}$ and small-scale quantity φ'. $\bar{\varphi}$ can be expressed as follows,

$$\bar{\varphi}(x) = \int_V \varphi(x')G(x,x')dx', x'\epsilon\forall, \quad (3)$$

in which φ is the original (unfiltered) function, x' is the spatial coordinate, x is the spatial coordinate after filtering, G is the filter function, V is the volume of a computational cell and $\forall$ is the computational domain [30]. The filter function is

$$G(x,x') = \begin{cases} \frac{1}{V}, x'\epsilon\forall \\ 0, x' \text{ otherwise} \end{cases} \quad (4)$$

Considering Newtonian fluid and compressible flow, the filtered mass and momentum equations are given by

$$\frac{\partial \rho}{\partial t} + \frac{\partial}{\partial x_i}(\rho \bar{u}_i) = 0, \tag{5}$$

$$\frac{\partial}{\partial t}(\rho \bar{u}_i) + \frac{\partial}{\partial x_j}\left(\rho \bar{u}_i \bar{u}_j\right) = \frac{\partial}{\partial x_j}\left(\sigma_{ij}\right) - \frac{\partial \bar{p}}{\partial x_i} - \frac{\partial \tau_{ij}}{\partial x_j} \tag{6}$$

In Eq. (6), σ_{ij} is the stress tensor due to molecular viscosity, defined as

$$\sigma_{ij} = \left[\mu\left(\frac{\partial \bar{u}_i}{\partial x_j} + \frac{\partial \bar{u}_j}{\partial x_i}\right)\right] - \frac{2}{3}\mu \frac{\partial \bar{u}_l}{\partial x_l}\delta_{ij}. \tag{7}$$

Further, ρ, u and p are fluid density, velocity and pressure, respectively. μ is the dynamic viscosity and τ_{ij} is the subgrid-scale stress tensor defined as

$$\tau_{ij} = \rho\overline{u_i u_j} - \rho \bar{u}_i \bar{u}_j. \tag{8}$$

Based on the Boussinesq hypothesis, the subgrid-scale turbulent stresses is computed as

$$\tau_{ij} - \frac{1}{3}\tau_{kk}\delta_{ij} = -2\mu_t \bar{S}_{ij}, \tag{9}$$

where $\bar{S}_{ij}$ is the strain rate tensor for the resolved scales and defined by

$$\bar{S}_{ij} \equiv \frac{1}{2}\left(\frac{\partial \bar{u}_i}{\partial x_j} + \frac{\partial \bar{u}_j}{\partial x_i}\right). \tag{10}$$

Various models have been introduced in the literature for subgrid-scale turbulent viscosity (μ_t) modelling. In the current study, Wall-Adapting Local Eddy-Viscosity (WALE) model [30] is adopted. This is due to the advantages of this model for wall bounded flows, particularly in comparison with the well-known Smagorinsky-Lilly model [31]. WALE considers zero turbulent viscosity for laminar shear flows in contrast with the Smagorinsky-Lilly model [31], which assumes non-zero turbulent viscosity. This allows WALE model to treat more correctly the laminar zones in the domain. In this model, μ_t is calculated from

$$\mu_t = \rho L_s^2 \frac{\left(S_{ij}^d S_{ij}^d\right)^{3/2}}{\left(\bar{S}_{ij}\bar{S}_{ij}\right)^{5/2} + \left(S_{ij}^d S_{ij}^d\right)^{5/4}}, \tag{11}$$

where $S_{ij}^d = \frac{1}{2}\left(\bar{g}_{ij}^2 + \bar{g}_{ji}^2\right) - \frac{1}{3}\delta_{ij}\bar{g}_{kk}^2$ and $\bar{g}_{ij} = \frac{\partial \bar{u}_i}{\partial x_j}$. L_s is the mixing length of the subgrid-scale and is computed by [30]

$$L_S = min\left(\kappa d, C_w V^{1/3}\right). \tag{12}$$

Details of L_S function can be found in Ref. [30].

The filtered energy equation results in the following equation

$$\frac{\partial \rho \bar{h}_s}{\partial t} + \frac{\partial \rho \bar{u}_i \bar{h}_s}{\partial x_i} - \frac{\partial \bar{p}}{\partial t} - \bar{u}_j \frac{\partial \bar{p}}{\partial x_i} - \frac{\partial}{\partial x_i}\left(\lambda \frac{\partial \bar{T}}{\partial x_i}\right) = -\frac{\partial}{\partial x_j}\left[\rho\left(\overline{u_i h_s} - \bar{u}_i \bar{h}_s\right)\right] = \frac{\partial}{\partial x_j}\left(\frac{\mu_{SGS} C_p}{Pr_{SGS}} \frac{\partial \bar{T}}{\partial x_j}\right), \tag{13}$$

where $\bar{h}_s$ and λ are the sensible enthalpy and thermal conductivity, respectively. The term $\rho\left(\overline{u_i h_s} - \bar{u}_i \bar{h}_s\right)$ is the subgrid enthalpy flux.

In Eq. (13), μ_{SGS} and Pr_{SGS} are subgrid viscosity and Prandtl number, respectively.

The governing equations are solved by the open-source CFD toolbox, OpenFOAM. The finite volume method, on a Cartesian grid, is adopted to solve the unsteady compressible Navier-Stokes equation with the coupled algorithm that solves the momentum and continuity equations together. The spatial discretization was performed using the second-order accurate and bounded. A second-order backward Euler transient scheme was applied for the time discretization [32]. The time step is chosen such that the Courant-Friedrichs-Lewy number (CFL) [33] becomes lower than unity. According to CFL definition, time step is taken to be

$$\Delta t = CFL\, \Delta x_{min}/u_{1\,max}, \tag{14}$$

in which Δx_{min} is the minimum grid width and $u_{1\,max}$ is the maximum longitudinal velocity. Each simulation was initialized with the solution of a preceding steady RANS simulation to achieve fast convergence of computation. Further, to assure obtaining reliable results, a time twice of channel washout of a massless particle is elapsed before recording the results.

2.3. Inlet entropy wave

By considering steady and perturbation parts of quantities in the first law of thermodynamics and assuming an ideal gas as well as the linearity of the perturbation (denoted by a prime) with respect to the steady part (denoted by an overbar), the following relation for entropy fluctuation can be written [34]:

$$\frac{s\prime}{c_p} = \frac{T\prime}{\bar{T}} - \left(\frac{\gamma-1}{\gamma}\right)\frac{p\prime}{\bar{p}} \quad (15)$$

In the absence of acoustic fluctuations (i.e. p' is negligible), it can be concluded that $\frac{s\prime}{c_p} \cong \frac{T\prime}{\bar{T}}$ [26], which shows that the temperature and entropy scales are similar. This is the rationale behind introducing the entropy wave by a transient temperature function at the inlet. Yet, it is essential to note that there is no linearization in this study. Temperature pulse is added to the air flow using a linear increment and an exponential decrement function [35]. Unlike the induced heat source function of Morgans et al. [26], this has the ability of practical implementation [35] and lower potential of overshoot numerical error. This high temperature region, with the amplitude of 1.1 times of the base flow temperature (in Kelvin), is then convected through the channel and forms the entropy wave.

2.4. Grid size and validation

To obtain an optimum grid size, two important parameters were computed. The ratio of area under temperature-time graph at the inlet to that at the outlet was first computed and compared for various grid sizes. The results showed a grid of 490000 cells was sufficiently fine to ensure a grid independent solution. This is determined by examining LES_IQ_k index [36] for various grid sizes. LES_IQ_k, defined as the following

$$LES\_IQ_k = \frac{k^{res}}{k^{tot}}, \quad (16)$$

is an assessment index for quality of a LES mesh size. Here, k^{res} is the resolved kinetic energy and k^{tot} the total kinetic energy. LES_IQ_k for most engineering applications that typically occur at high Reynolds numbers is adequate in the range of 0.75 to 0.85 [37]. The minimum LES_IQ_k in the current study was 91%, which confirms that this number of cells assured grid independency. The grid, further, should be fine near walls; thus, dimensionless velocity (u^+) and wall distance (y^+) for turbulent flow are secondly considered,

$$u^+ = \frac{U}{u_\tau}, y^+ = \frac{\rho u_\tau \Delta y}{\mu}, \quad (17)$$

in which Δy is the distance of the cell from the wall and U is the time-averaged velocity. u^+ versus y^+ graph in Fig. 2 shows that the current grid ensures a good coincidence against DNS results of Moser et al. [38]. Further, y^+ for the nearest cell to the wall is less than unity (about 0.9 which is not presented in this figure), as recommended by LES developers [31].

Take in Fig. 2

Physical diffusion is of high significance in this study, as it determines dispersion and dissipation of the entropy wave. Conductivity and viscosity are two sources of thermal and inertial physical diffusion, involved in energy and momentum equations, respectively. Numerical diffusion, however, may act as a non-physical source that affects the results. Although second-order discretization and fine grid size reduce the importance of numerical diffusion in the current study, this should be still examined in an Eulerian flow. To evaluate the numerical diffusion of the simulations, an inviscid flow with zero thermal conductivity was assumed. The inlet temperature of the flow was 300K. The entropy wave was induced at the inlet. Fig. 3 shows the ratio of mass-weighted average of temperature increment to the base temperature in various cross-sections. This figure shows that the behavior of the wave remains overall unchanged. There is a minor difference in the area under the graph, as an index of wave dissipation, between the inlet and the outlet. Further, the maximum change of the wave width, as an index of wave dispersion, is about 3 percent. Numerical diffusion is, therefore, negligible and it can be claimed that diffusion found in the simulation is exclusively of physical nature.

Take in Fig. 3

Finally, the temperature increment versus time, which represents the entropy wave, was compared favorably with the experimental results of Bake et al. [35]. This experiment included temperature measurement, by only one thermocouple, in the so called entropy wave generator. The setup included a duct equipped with an unsteady electrical heater as the source of entropy waves. Once generated, the waves were convected downstream and passed through the inserted thermocouples before entering a downstream nozzle [35]. Due to the unknown spanwise and altitudinal position of the thermocouple in Ref. [35], mass-weighted average of temperature against experimental data of Ref. [35] is illustrated in Fig. 4. This is the reason for the existence of small difference between the two sets of data at the wave rear. Near channel walls region is included in mass-weighted average of the numerical work, but not in the experimental data of Ref. [35]. The slower mean velocities near the channel walls causes a spreading of the back of the temperature pulse [26]. Except for some small discrepancies at the back of the pulse, good coincidence is observed in Fig. 4. It should be further noted that the results of the current numerical simulations were also compared with DNS of Jongwoo and Yoo [39] on mixed thermal convection. This resulted in excellent agreements for the velocity profiles and average Nusselt number variations.

Take in Fig. 4

3. Results and discussion

As stated earlier, entropy waves are subject to some levels of dissipation which can potentially affect combustor hydrodynamics. For a fixed amplitude of temperature disturbance, Reynolds number (Re) and turbulence intensity (TI) are considered as the governing inlet parameters. Further, as argued earlier, thermal boundary conditions are important in this topic. In the current work, two thermal boundary conditions are considered. These include the convective and adiabatic conditions on the walls. The thermal properties of convective heat transfer on the external walls are stated earlier in section 2.1. The former is a more realistic boundary condition in gas turbine combustors and the latter has been used in the previous studies of entropy waves [26]. The investigated test cases are listed in Table 1.

Take in Table 1

The snapshot of $\Delta T/T_{base}$ for the wave convecting through the channel is depicted in Figs. 5 and 6. It should be noted that temperature ranges of Figs. 5 and 6 are slightly different due to different effects of thermal boundary conditions. In these figures, the left column correspond to the situations, in which the wave has just completely entered the duct and the inlet has the base flow temperature. The right column, however, shows a later moment, when the whole wave is still flowing in the channel and thus, the outlet has the base flow temperature. Dissipation of the wave is clear in these figures. This is especially true, for $0.5Re_{max}$ cases (even number cases) compared with those of Re_{max} (odd number cases) and is primarily due to the lower bulk flow velocity, which makes the waves more exposed to annihilation mechanisms of the flow. On the other hand, in Re_{max} cases, although the turbulence effect is high, convecting velocity of the wave is also higher rendering a shorter residence time of the wave and therefore less time for being influenced. Similar effects of bulk velocity on the wave front deformation have been reported in convecting reactive waves [40]. The slower velocity near the walls results in stronger dissipation of the wave in this region. Further, the wave dissipation in cases with convective heat transfer on the walls is considerable which may arise from both hydrodynamic and thermal effects. It is also observed in Figs. 5 and 6 that higher *TI* (cases 3, 4, 7 and 8) has, generally, resulted in more significant wave dissipation. This is found by thinner hot core of the wave at the outlet. The snapshots show that as a result of wave dissipation, heat diffuses into the base flow. This, in turns, leaves some influences on the hydrodynamics of the channel flow as evaluated in this section.

Take in Fig.5 and Fig. 6

Table 2 shows the ratio of the medium enthalpy difference before entrance of the wave and just after washing the wave out of the channel (when the wave rear increases the base flow temperature by 10 percent at the channel exit) for the whole channel to the enthalpy of the wave. Only adiabatic cases are shown in Table 2. This ratio represents the fraction of the thermal energy of the entropy wave, which diffused into the base flow. The values presented in Table 2 might seem to be negligible. Nevertheless, as the results in this section show, such low values can still considerably affect the vorticity field. The ratio increases by increasing TI or decreasing Re . The snapshots in Fig. 5 indicate that Re has a very noticeable deterioration effect on the waves. Yet, the results of Table 2 express that TI leaves a relatively stronger effect on the thermal diffusion of wave. Nonetheless, it is important to note that this comparison is only valid in the considered range of Re and TI.

Take in Table 2

To quantify hydrodynamic modification caused by the convection of the entropy wave, some metrics are introduced in this study. One of the main parameters characterizing the hydrodynamics of all flows is vorticity. In combustors, vorticity is of particular significance due its direct pertinence to the mechanism of vortex sound [17]. This is an aerodynamic noise generation mechanism, which can have similar undesirable consequences to those of entropy noise [17]. To evaluate vorticity modifications the following metrics are used; integration of absolute vorticity, local spanwise vorticity and local streamwise vorticity. The effectiveness of these has been previously in the field bio-fluid dynamics [41,42].

Average integration of absolute vorticity ($AIAV$) magnitude upon spatial and temporal domains is firstly presented, as the following

$$AIAV = \frac{1}{\forall \Delta t} \iint \omega d\forall dt. \tag{18}$$

In Eq. (18), $\forall$ is the channel volume and Δt is the time taken for washing a massless particle out the channel for the case without an entropy wave and the time of entropy wave convecting through the channel for the case with an entropy wave. Fig. 7 illustrates that $AIAV$ decreases after passage of the wave throughout the channel. Although convection of the wave results in a low increment of the enthalpy ratio (see Table 2), it leaves up to 50 percent reduction in $AIAV$ (see Fig. 7). This is probably due to increasing kinematic viscosity and decreasing density in the gas medium. An increase in Re or TI, further, raises $AIAV$. TI can increase $AIAV$ with a factor 8. Re, however, has a lower effect, as this increases $AIAV$ up to 200 percent. The effect of entropy wave on $AIAV$ is more pronounced at higher TI in convective wall cases, while this is more highlighted at lower TI in the adiabatic cases.

Take in Fig. 7

The magnitudes of velocity ($\vec{V}$) and vorticity ($\vec{\omega}$) vector, as well as the angle between them are of importance in the description of a flow field. The inner product of the velocity and vorticity vectors, called helicity, is used to characterize complex fluid flows as a measure of fluid dynamical quantity, which shows the degree to which the streamlines wrap and coil around each other [43]. Similar to energy, helicity has a great influence on the evolution and stability of turbulent and laminar flows and is defined as [44]

$$Helicity = \vec{V}.(\vec{\nabla} \times \vec{V}). \tag{19}$$

Considering Eq. (19), Grigioni et al. [41] defined the basic quantity,

$$\Psi\big(s(t)\big) = \frac{\vec{V}.(\vec{\nabla}\times\vec{V})}{\vec{V}|\vec{\nabla}\times\vec{V}|} = \cos\varphi. \tag{20}$$

Ψ is a normalized function of helicity, varying between 0 and 1, for purely axial or circumferential and purely helical flow, respectively. φ is the angle formed between velocity and vorticity vectors.

Fig. 5 shows the averaged integration of absolute helicity ($AIAH$) upon spatial and temporal domain, described as follows.

$$AIAH = \frac{1}{\forall \Delta t} \iint \vec{V}.(\vec{\nabla} \times \vec{V}) d\forall dt, \tag{21}$$

$\forall$ and Δt are the same as those defined in Eq. (18). Affected by the vorticity magnitude (see $AIAV$ values), $AIAH$ signifies with increasing either of Re or TI. Fig. 8 further shows the strong influence of TI on $AIAH$. This is such that, in some cases, variations in TI can alter $AIAH$ by a factor 8, which is the same increment in $AIAV$. It is also observed in Fig. 8 that $AIAH$ is much lower in cases with small TI compared with those of high TI. Further, the effect of entropy wave on variation of $AIAH$ is more intensified at adiabatic cases compared with those of convective heat transfer. Similar to $AIAV$, convection of entropy waves causes a reduction in $AIAH$, which is up to 50 percent. Fig. 9 indicates that the averaged integration of absolute Ψ ($AIAS$, see Eq. (22)) presents a similar variation of $AIAH$ as that found in Fig. 8. Nevertheless, due to the same order of magnitude of $AIAH$ and $AIAV$, $AIAH$ is mainly affected by the vorticity values rather than Ψ.

$$AIAS = \frac{1}{\forall \Delta t} \iint \Psi d\forall dt, \tag{22}$$

Fig. 11 further, illustrates that the passage of entropy wave results in more streamlines wrapping, while increasing either of Re or TI enhances streamline coiling. Due to the axial flow in the channel, $AIAS$ takes a low value. Entropy wave imparts weaker effect on $AIAS$, in comparison with the other indices. For instance, in Figs. 8 and 9, entropy wave can raise $AIAH$ by 200 percent, while $AIAS$ is altered not more than 100 percent. The preceding analyses show that the hydrodynamic modifications are most pronounced for the adiabatic channel with Re_{max} and TI=5% and the thermally convective channel with $0.5Re_{max}$ and TI=20%. This result, once again, emphasizes the significance of thermal boundary conditions in the annihilation process of entropy waves.

Take in Fig. 8 and Fig. 9

Using helicity definition, it is possible to define two basic quantities; the local streamwise vorticity ($STWV$), and the local spanwise vorticity ($SPWV$) [42], defined as the following,

$$STWV = \frac{\vec{V}.\vec{\omega}}{|\vec{V}|} = |\vec{\omega}| cos\varphi, \tag{23}$$

$$SPWV = \frac{\vec{V}\times\vec{\omega}}{|\vec{V}|} = |\vec{\omega}| sin\varphi = |\vec{\omega}| \sin[cos^{-1}\Psi]. \tag{24}$$

By a particle-trace analysis new metrics can be introduced [42] that give a measure of the alignment of the local velocity and vorticity vectors. Over the trajectory described by the generic particle labeled k moving through the channel, the following quantities can be calculated.

$$stwvi_k = \frac{1}{N_k}\sum_{j=1}^{N_k}\left|STWV_{k,j}\right|, \tag{25}$$

$$spwvi_k = \frac{1}{N_k}\sum_{j=1}^{N_k}\left|SPWV_{k,j}\right|, \tag{26}$$

where N_k is the number of points j (j=1,.., N_k) in the kth trajectory (k=1,.., N_{path}) in which $STWV$ and $SPWV$ are calculated. Further, the streamwise vorticity index ($STWVI$) and the spanwise vorticity index ($SPWVI$) are defined as follows [42]

$$STWVI = \frac{1}{N_{path}}\sum_{k=1}^{N_{path}} stwvi_k = \frac{1}{N_{path}}\sum_{k=1}^{N_{path}}\frac{1}{N_k}\sum_{j=1}^{N_k}\left|STWV_{k,j}\right|, \tag{27}$$

$$SPWVI = \frac{1}{N_{path}}\sum_{k=1}^{N_{path}} spwvi_k = \frac{1}{N_{path}}\sum_{k=1}^{N_{path}}\frac{1}{N_k}\sum_{j=1}^{N_k}\left|SPWV_{k,j}\right|. \tag{28}$$

In this study, a cluster of massless, neutrally buoyant, non-diffusing particles [41] (N_{path}=50) are injected uniformly at the channel inlet. 100 points are then considered (N_k=100) with the same spatial intervals on the particle paths through the channel.

Figs. 10 and 11 demonstrate the values of $STWVI$ and $SPWVI$ for the investigated test cases. Similar to the other studied parameters, increasing Re or TI has a signifying effect on $STWVI$. This is due to increasing both vorticity (as $AIAV$ illustrates in Fig. 7) and cosine of angle between the velocity and vorticity vector, Ψ, (as $AIAS$ represents in Fig. 9). Although sine of φ decreases by raising Re or TI, $SPWVI$ increases due to the dominant influence of vorticity magnitude. The value of $STWVI$ is much smaller than $SPWIVI$, which is clear from the low values of Ψ (found from $AIAS$). Entropy waves have a diminishing effect on both $STWVI$ and $SPWVI$. Figs. 10 and 11 further reveal that entropy waves can change the alignment of the local velocity and vorticity vectors by passing through the channel. The effect of entropy wave on $STWVI$ is stronger at adiabatic cases, while its effect on

$SPWTVI$ is more pronounced at convective cases. Similar to that discussed in Figs. 7-9, the strongest effects of entropy waves on hydrodynamics is found at Re_{max} and TI=5% for the adiabatic channel and, $0.5Re_{max}$ and TI=20% for the thermally convective channel.

The presented results clearly show that in contrast to the existing view [26], entropy waves or hot spots are not passive scalars. Isolation of them from the base flow can be therefore questionable and leads to faulty prediction of a combustor hydrodynamics.

Take in Fig. 10 and Fig. 11

4. Conclusions

This paper presented a numerical study on the effects of the annihilation of entropy waves upon the combustor hydrodynamics. To establish quantitative measures of these effects, some hydrodynamic indices were introduced. Most of these indices were associated with vorticity, due to the direct impact of vorticity on the hydrodynamics and the mechanism of vortex sound generation. Adiabatic walls, as a usual thermal boundary condition, and convective walls, as a realistic and rarely investigated thermal boundary condition were considered. Large eddy simulation of the flow between two parallel plates, in which entropy waves are convected, showed that entropy waves can considerably modify the channel hydrodynamics.

The main findings of this work can be summarized as follows.

- Convection of the entropy wave causes up to 50 percent reduction in average integrations of absolute vorticity and helicity.
- Passage of entropy wave results in more streamlines wrapping, while increasing either of Re or TI leads to stronger streamlines coiling.
- Flow in the channel with convective heat transfer on the walls causes more annihilation on the passing entropy wave, compared with that in the case with adiabatic walls.
- Convection of the entropy waves can change the alignment of the local velocity and vorticity vectors; this is more highlighted in adiabatic cases.
- Average integration of absolute helicity is mainly dominated by vorticity rather than the angle between vorticity and velocity.
- The strongest influences of entropy waves on the channel hydrodynamics was found at Re_{max} and TI=5% of the adiabatic channel and $0.5Re_{max}$ and TI=20% of the thermally convective channel.

These results clearly showed that in contrast to the existing view, entropy waves or hot spots are not passive scalars and isolation of them from the base flow can be questionable. The presented analyses in this work, further, demonstrated the considerable effect of the annihilation of entropy waves on the flow vorticity field. They showed that the decaying entropy waves can signify flow vortices, which can potentially contribute with the aerodynamic sound generation.

References

[1] S. Candel, D. Durox, S. Ducriux, A. Birbaud, N. Noiray, D. Schuller, Flame dynamics and combustion noise: progress and challenges, Aeroacoustics 8.1&2(2009) 1-56.

[2] S. Candel, D. Durox, T. Schuller, N. Darabiha, L. Hakim, T. Schmitt, Advances in combustion and propulsion applications, European Journal of Mechanics-B/Fluids 40 (2013) 87-106.

[3] ACARE Aeronautics and air transport: beyond vision 2020 (towards 20150), European Union, 2010

[4] T. C. Lieuwen, Unsteady combustor physics, Cambridge University Press, 2012.

[5] N. A. Cumpsty, F. E. Marble, The interaction of entropy fluctuations with turbine blade rows; a mechanism of turbojet engine noise, Proceedings of the Royal Society of London A: Mathematical, Physical and Engineering Sciences 357.1690 (1977) The Royal Society.

[6] I. Duran, S. Moreau, Solution of the quasi-one-dimensional linearized Euler equations using flow invariants and the Magnus expansion, Journal of Fluid Mechanics 723 (2013) 190-231.

[7] J. H. Miles, Time delay analysis of turbofan engine direct and indirect combustion noise sources, Journal of Propulsion and Power 25.1 (2009) 218-227.

[8] P A. Hield, M J. Brear, S H. Jin, Thermoacoustic limit cycles in a premixed laboratory combustor with open and choked exits. Combustion and Flame 156.9 (2009) 1683-1697.

[9] JE. Ffwocs Williams, M. Howe, The generation of sound by density inhomogeneities in low Mach number nozzle flows, Journal of Fluid Mechanics 41(1975) 207-232.
[10] M. Howe, Contributions to the theory of aerodynamic sound, with application to excess jet noise and the theory of the flute, Journal of Fluid Mechanics 71(1975) 625-673.
[11] FE. Marble, SM. Candel, Acoustic Disturbances From Gas Non-Uniformities Convected Through a Nozzle, Journal of Sound and Vibration 55.2(1977) 225-243.
[12] SR. Stow, AP. Dowling, TP. Hynes, Reflection of circumferential modes in a choked nozzle, Journal of Fluid Mechanics 467(2002) 215-239.
[13] CS. Goh, AS. Morgans, Phase prediction of the response of choked nozzles to entropy and acoustic disturbances, Journal of Sound and Vibration 330(2011) 5184-5198.
[14] WH. Moase, MJ. Brear, C. Manzie, The forced response of choked nozzles and supersonic diffusers, Journal of Fluid Mechanics 585(2007) 281-304.
[15] MJ. Brear, DC. Carolan, N. Karimi, Dynamic response of the exit nozzle of a premixed combustor to acoustic and entropic disturbances, The 8th European Fluid Mechanics Conference, Bad Reichenhall: Germany, 2010.
[16] NA. Cumpsty, Marble FE. Core noise from gas turbine exhausts. Journal of Sound and Vibration 1977;54(2):297-309
[17] Cumpsty NA. Jet Engine Combustion Noise: Pressure, Entropy and Vorticity Perturbations Produced by Unsteady Combustion or Heat Addition. Journal of Sound and Vibration 66.4(1979) 527-544.
[18] M. Talei, ER. Hawkes, M. Brear, A direct numerical simulation study of frequency and Lewis number effects on sound generation by two-dimensional forced laminar premixed flames, Proceedings of the Combustion Institute Proceedings of the Combustion Institute 34.1 (2013) 1093-1100.
[19] M. Talei, MJ. Brear, ER. Hawkes, A comparative study of sound generation by laminar, combusting and non-combusting jet flows, Theoretical and Computational Fluid Dynamics 28(2014) 385-408.
[20] N. Karimi, Response of a conical, laminar premixed flame to low amplitude acoustic forcing- A comparison between experiment and kinematic theories, Energy 78(2014) 490-500.
[21] AV. Singh, A. Eshaghi, M. Yu, AK. Gupta, KM. Bryden, Pollutant emission and noise radiation from open and impinging inverse diffusion flames, Applied Energy 115(2014) 116-127.
[22] HS. Zhen, YS. Choy, CW. Leung, C S. Cheung, Effects of nozzle length on flame and emission behaviors of multi-fuel-jet inverse diffusion flame burner, Applied Energy 88.9(2011) 2917-2924.
[23] J. Eckstein, E. Freitag, C. Hirsch, T. Sattelmayer, Experimental study on the role of entropy waves in low-frequency oscillations in a RQL combustor, Journal of engineering for gas turbines and power 128.2(2006) 264-270.
[24] J. Eckstein, T. Sattelmayer, Low-Order Modeling of Low-Frequency Combustion Instabilities in Aeroengines, Journal of Propulsion Power 22.2 (2006) 425-432.
[25] T. Sattelmayer, Influence of the combustor aerodynamics on combustion instabilities from equivalence ratio fluctuations. Journal of Engineering Gas Turbines Power 125 (2003) 11-20.
[26] AS. Morgans, CS. Goh, JA. Dahan, The dissipation and shear dispersion of entropy waves in combustor thermoacoustics. Journal of Fluid Mechanics 733(2013) R2-1-R2-11.
[27] N. Karimi, M. Brear, W. Moase, Acoustic and disturbance energy analysis of a flow with heat communication. Journal of Fluid Mechanics 597(2008) 67-89.
[28] White, Frank M. "Fluid mechanics, WCB." ed: McGraw-Hill, Boston (1999), chapter 6.
[29] A. H. Lefebvre, Gas turbine combustion. CRC press, 1998.
[30] F. Nicoud, F. Ducros, Subgrid-Scale Stress Modelling Based on the Square of the Velocity Gradient Tensor.Flow, Turbulence, and Combustion. 62.3(1999) 183-200.
[31] J. Smagorinsky, General Circulation Experiments with the Primitive Equations: I. The Basic Experiment, Month.Wea. Rev. 91 (1963) 99-164.

[32] F. Bake, et al. The entropy wave generator (EWG): a reference case on entropy noise, Journal of Sound and Vibration 326.3 (2009) 574-598.
[33] F. Jorg, et al. The COST 732 Best Practice Guideline for CFD simulation of flows in the urban environment: a summary, International Journal of Environment and Pollution 44.1-4 (2011) 419-427.
[34] C. Boa-The, On the energy transfer to small disturbances in fluid flow (Part I), Acta Mechanica 1.3 (1965) 215-234.
[35] F. Bake, N. Kings, I. Roehle, Fundamental mechanism of entropy noise in aero-engines: Experimental investigation, Journal of Engineering for Gas Turbines and Power 130.1 (2008) 011202-1-8.
[36] S. B. Pope, Turbulent flows, Cambridge University Press, New York, 2000.
[37] [b] I. B. Celik, Z. N. Cehreli, I. Yavuz. Index of resolution quality for large eddy simulations. Journal of fluids engineering 127.5 (2005) 949-958.
[38] J. K. R. D. Moser, N. N. Mansour, Direct numerical simulation of turbulent channel flow up to ReÄ590, American Institute of Physics 11.4 (1999) 943-945.
[39] Y. Jongwoo, JY. Yoo, H. Choi, Direct numerical simulation of heated vertical air flows in fully developed turbulent mixed convection, International Journal of heat and mass transfer 46.9 (2003) 1613-1627.
[40] L. Rongy et al. Influence of thermal effects on buoyancy-driven convection around autocatalytic chemical fronts propagating horizontally. Chaos: An Interdisciplinary Journal of Nonlinear Science. 19.2 (2009) 023110-1-7.
[41] G. Mauro, et al. A mathematical description of blood spiral flow in vessels: application to a numerical study of flow in arterial bending, Journal of biomechanics 38.7 (2005) 1375-1386.
[42] M. Umberto, et al. Blood damage safety of prosthetic heart valves. Shear-induced platelet activation and local flow dynamics: A fluid–structure interaction approach, Journal of biomechanics 42.12 (2009) 1952-1960.
[43] HK. Moffatt, The degree of knottedness of tangled vortex lines J. Fluid Mech 35.1 (1969) 117-129.
[44] A. Belian, et al. Helical turbulence: turbulent viscosity and instability of the second moments, Physica A: Statistical Mechanics and its Applications 258.1 (1998) 55-68.

Table 1- Case studies explanation

Case No.	Description
1	Re_{max} , TI=5%, Adiabatic walls
2	0.5Re_{max} , TI=5%, Adiabatic walls
3	Re_{max} , TI=20%, Adiabatic walls
4	0.5Re_{max} , TI=20%, Adiabatic walls
5	Re_{max} , TI=5%, Convective walls
6	0.5Re_{max} , TI=5%, Convective walls
7	Re_{max} , TI=20%, Convective walls
8	0.5Re_{max} , TI=20%, Convective walls

#

Table 2- The ratio of the enthalpy difference before entrance of the wave and just after the wave washing out of the channel for the whole channel to enthalpy of the wave

#Case No.	(Enthalpy difference before entrance of the wave and just after the wave washing out of the #channel)/Enthalpy of the wave)
1	#0.612 %
2	0.646 %
3	0.666 %
4	0.703 %

1

2

#

3

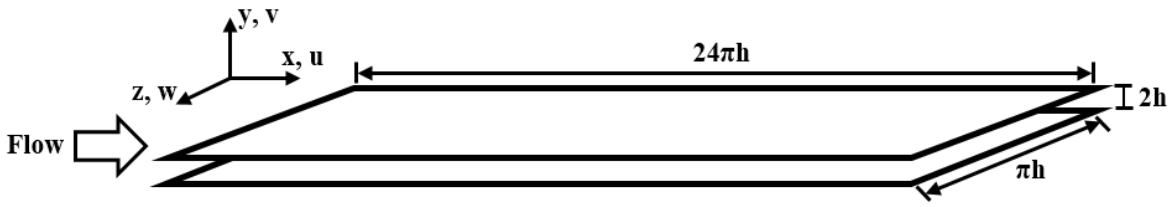

Fig. 1. Schematic configuration of the channel.

#

4

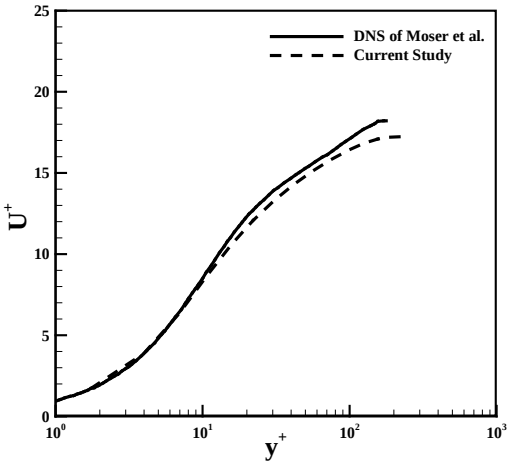

Fig. 2. Dimensionless velocity versus wall distance: a comparison between the current LES and DNS of Moser et al. [38].

#

5

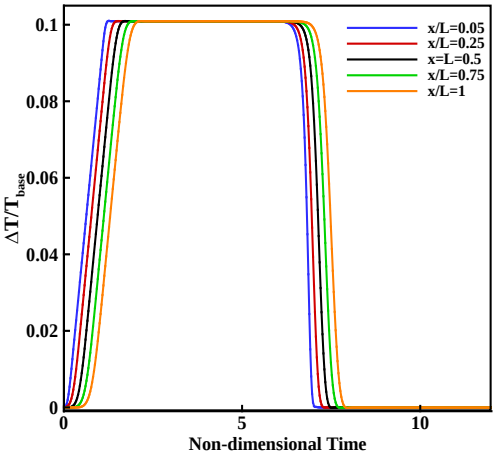

Fig. 3. The ratio of increment to the base temperature value in various cross-sections of an Eulerian flow.

#

#

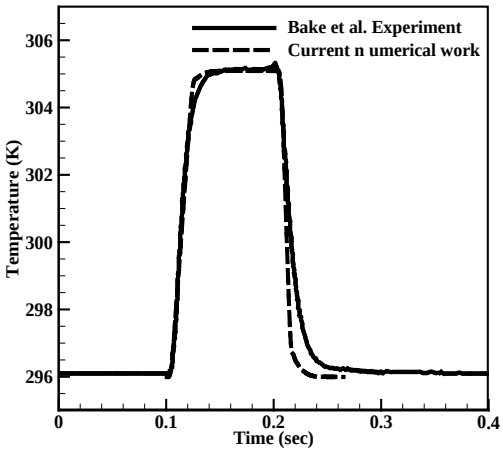

Fig. 4. Temperature increment as the entropy wave versus time: a comparison between the current numerical study and experiments of Bake et al. [35].

#

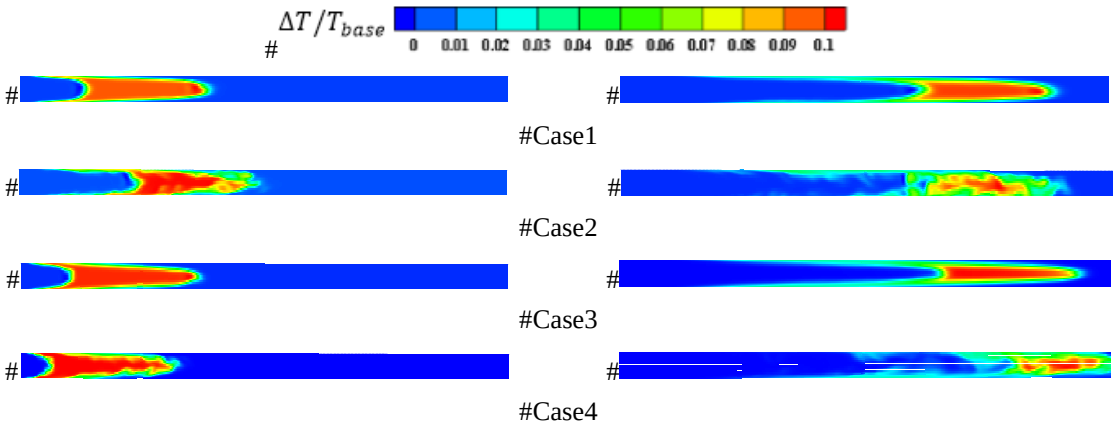

#Fig. 5. Snapshot of $\Delta T/T_{base}$ for the wave convecting through the channel with adiabatic walls.

#

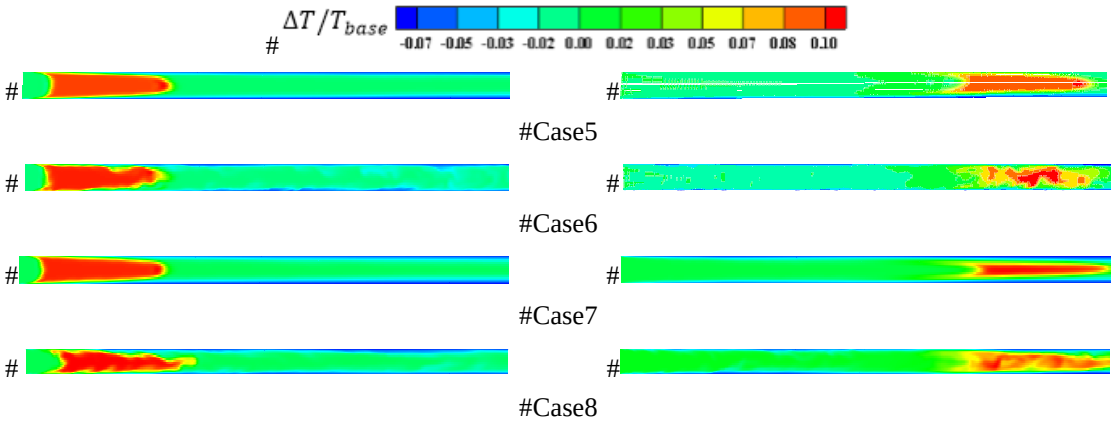

Fig. 6. Snapshot of $\Delta T/T_{base}$ for the wave convecting through the channel with thermally convective walls.

#

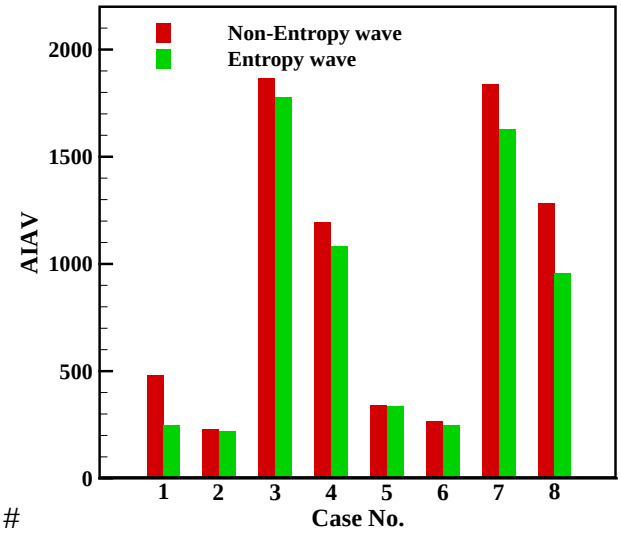

Fig. 7. Average integration of absolute vorticity upon volume and time for cases with and without entropy wave convecting through the channel.

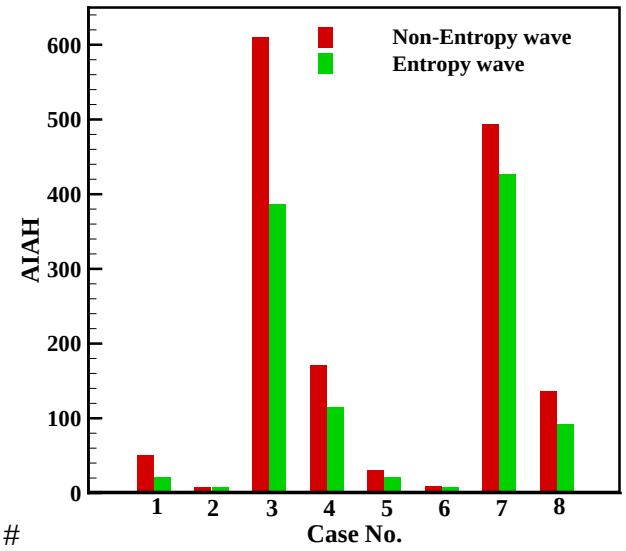

Fig. 8. Averaged integration of absolute helicity upon volume and time for the cases with and without entropy wave convecting through the channel.

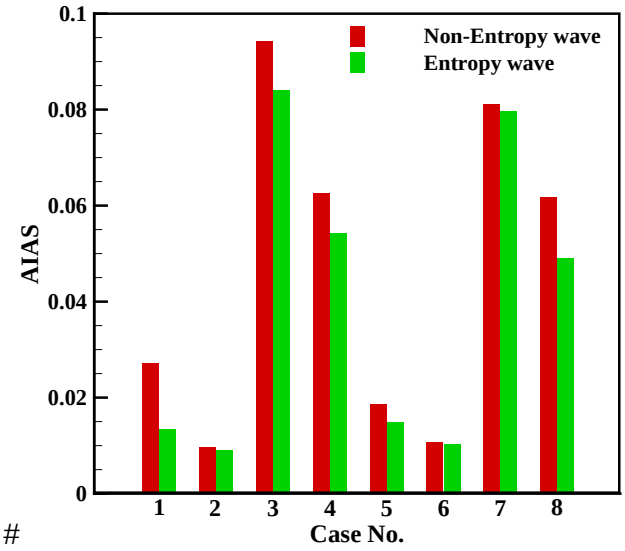

Fig. 9. Averaged integration of absolute Ψ upon volume and time for the cases with and without entropy wave convecting through the channel.

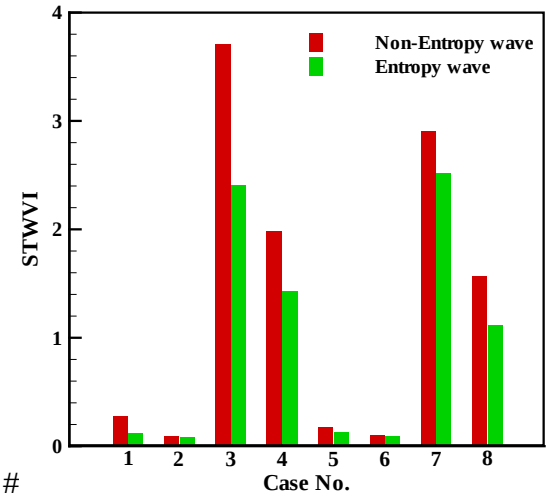

Fig. 10. *STWVI* for the cases with and without entropy wave convecting through the channel.

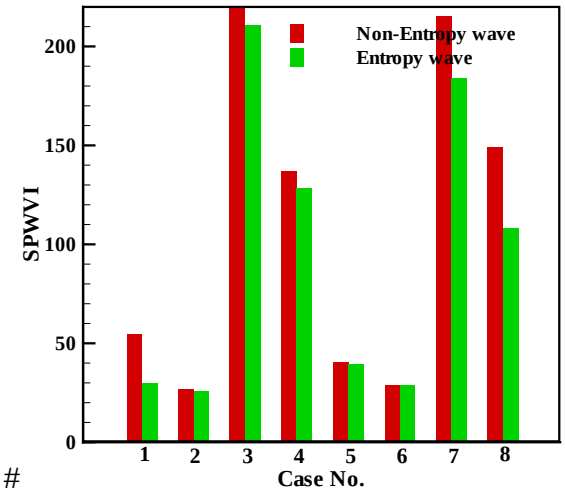

Fig. 11. *SPWVI* for studied cases with and without entropy wave convecting through the channel.